Dalton Transactions

Accepted Manuscript

ROYAL SOCIETY OF CHEMISTRY

www.rsc.org/dalton

Structure and Efficient Luminescence Upconversion of Ln(III) Aromatic N-Oxide Coordination Polymers

Bowie S. K. Chong and Evan G. Moore*

A series of lanthanide-based coordination polymers $\{[Yb_{1-x}Er_x(4,4'\text{-bpdo})_3(H_2O)_2](CF_3SO_3)_3\}_\infty$ were synthesised by solvent diffusion techniques, where 4,4'-bpdo = 4,4'-bipyridine-*N,N'*-dioxide, and using differing mole fractions of Yb(III) and Er(III) which were systematically varied (x = 0, 0.05, 0.20, 0.50 and 1). All of the materials obtained were characterised using elemental analyses, single-crystal X-ray diffraction (SXRD) and solid-state photoluminescence studies. Structurally, the coordination polymers crystallise as an isomorphous series of infinite 2D sheets, which contain two inner sphere water molecules, and are isostructural with a previously characterised homometallic Yb(III) compound. In addition to the normal Near Infra-Red (NIR) luminescence, these compounds also demonstrate upconversion emission upon 980 nm excitation. Upconversion luminescence measurements reveal visible emission in the red, green, and blue regions corresponding to the $^2H_{11/2} \rightarrow {}^4I_{15/2}$, $^4F_{9/2} \rightarrow {}^4I_{15/2}$ and $^2H_{9/2} \rightarrow {}^4I_{15/2}$ transitions of the Er(III) cation upon two and three-photon excitation. We also observed weak emission from the Er(III) cation in the UV region for the first time in a Ln-MOF based material.

1. Introduction

Continuing research into the development of photovoltaic materials for solar energy conversion is of undeniable importance to facilitate a transition towards cleaner and more sustainable environmental practices. Over the last 20 years, significant advances in power conversion have been achieved, with dye-sensitised solar cells (DSSCs) reaching efficiencies of 12%,[1] bulk heterojunction solar cells achieving efficiencies of 11%[2] and crystalline silicon based devices approaching efficiencies as high as 25.6%.[3] Nonetheless, the majority of these devices waste large amounts of incident radiation below their absorption bandgap, with only 20-30% of photons able to be utilised to generate electricity.[4] Low energy Near-Infra Red (NIR) photons, making up ca. 50% of sunlight at the Earth's surface, pass through devices without being used.[5-6]

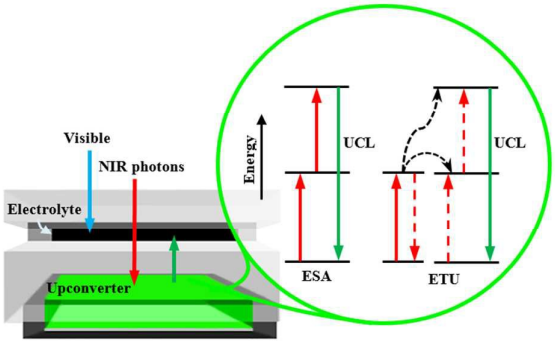

Figure 1. Layout of an upconversion-assisted photovoltaic device, and insert showing Excited State Absorption (ESA) and Energy Transfer Upconversion (ETU) processes occurring in Er^{3+}/Yb^{3+} doped complexes.

In order to reduce the spectral mismatch and improve conversion efficiency, non-linear optical processes such as photon upconversion (UC) offer a promising solution, allowing low-energy NIR radiation to be converted into higher energy Visible and/or UV photons,[7] which can then be redirected back towards the solar cell (Fig 1).

Not surprisingly, UC phenomena in crystalline and amorphous materials have been extensively studied over the last few decades, with many examples utilising the rich electronic structures of trivalent Ln(III) cations for applications in lasers,[8] optical waveguides[9] and biosensors.[10] Of these materials, $NaYF_4$ doped with Er^{3+} or co-doped with Yb^{3+} and Er^{3+} remains one of the most efficient UC phosphors.[11-13] Considerably less attention has been focused on upconverting luminescent lanthanide-based coordination polymers, despite the well-recognised structural diversity and luminescence properties of this class of materials,[14-16] with only a limited number of upconverting systems having been reported.[17-24] It has been noted elsewhere[24] that this may be due to the presence of multiphonon relaxation pathways in these materials, which could decrease the efficiency of the upconversion process.

Herein, we report the construction of bimetallic coordination polymers from a simple bis(unidentate) O-donor ligand, 4,4'-bipyridine-*N,N*'-dioxide (4,4'-bpdo), incorporating trivalent Yb^{3+} as a sensitiser for upconverted Er^{3+} emission. The high affinity of the trivalent lanthanide cation for the oxygen donor atoms ensures stability in the resulting materials, which form an isostructural and isomorphous high connectivity ($4^8 \cdot 6^2$) 2D network, the dimensions of which can be modified by altering the mole fraction of the incorporated metal ions. Interestingly, despite the presence of two coordinated inner sphere water molecules, we demonstrate efficient UC in these materials,

*School of Chemistry and Molecular Biosciences, The University of Queensland, Brisbane, QLD 4072, Australia. E-mail: egmoore@uq.edu.au; Fax: +61 (0) 7 3365 4273; Tel: +61 (0) 7 3365 3862

†Electronic supplementary information (ESI) available: CCDC 1478821-1478825. Additional details of crystallographic analysis and NIR emission spectra. For ESI and crystallographic data in CIF or other electronic format see DOI: xx.xxx/xxxxxx

with red and green emission observed upon low power NIR irradiation at 980 nm. Furthermore, we demonstrate that selective doping of differing mole fractions of metal cation can allow the luminescence upconversion mechanism to be fine-tuned in the visible and UV regions.

2. Experimental

2.1. General

All chemicals were purchased from commercial suppliers (Sigma Aldrich, Alfa Aesar) and were used without further purification unless stated otherwise. Solvents were dried using a Pure Solv™ purification system prior to use. High purity $Ln(CF_3SO_3)_3 \cdot xH_2O$ metal salts (Ln = Yb or Er, $x = 6$) were used in all metal complexation reactions.

2.2. Synthesis of the Bimetallic Complexes

The required 4,4'-bipyridyl-*N,N'*-dioxide (4,4'-bpdo), ligand was prepared using literature procedures[25] and metal complexation and crystallisations were performed using established solvent diffusion techniques.[26] Briefly, a homogenised mixture of solid Ln(III) salts (0.06 mmol) in various mole ratios from 0.0 (i.e. 100% Yb) to 1.0 (i.e. 100% Er) were placed at the bottom of a 20 mL glass vial and were covered with a halogenated anti-solvent (CH_2Cl_2, *ca.* 10 mL). A solution of the 4,4'-bpdo ligand (0.22 mmol) in MeOH (*ca.* 10 mL) was then carefully layered over the halogenated anti-solvent. Over a period of *ca*. 3-4 weeks, the solid metal salts gradually dissolved in the solvent mixture with concomitant formation of crystalline products at the solvent interface on the wall of the vial. Single crystals suitable for structural analysis were selected and analysed by X-ray diffraction, while elemental analysis (CHNS) was used to ensure sample homogeneity.

$\{[Yb(4,4'\text{-bpdo})_3(H_2O)_2](CF_3SO_3)_3\}_\infty \cdot 2H_2O$ (**1**)
Yellow crystals, Anal. Calc'd. (%) C 31.54, H 2.57, N 6.69, S 7.65; Found C 31.68, H 2.71, N 6.53, S 7.47 for $Yb_{1.0}C_{33}H_{32}N_6O_{19}F_9S_3$

$\{[Yb_{0.95}Er_{0.05}(4,4'\text{-bpdo})_3(H_2O)_2](CF_3SO_3)_3\}_\infty \cdot 3H_2O$ (**2**)
Yellow crystals, Anal. Calc'd. (%) C 31.10, H 2.69, N 6.59, S 7.55; Found C 31.00, H 2.54, N 6.49, S 7.38 for $Yb_{0.95}Er_{0.05}C_{33}H_{34}N_6O_{20}F_9S_3$

$\{[Yb_{0.8}Er_{0.2}(4,4'\text{-bpdo})_3(H_2O)_2](CF_3SO_3)_3\}_\infty \cdot 2H_2O$ (**3**)
Yellow crystals, Anal. Calc'd. (%) C 31.07, H 2.84, N 6.59, S 7.54; Found C 31.42, H 2.56, N 6.49, S 7.48 for $Yb_{0.8}Er_{0.2}C_{33}H_{32}N_6O_{19}F_9S_3$

$\{[Yb_{0.5}Er_{0.5}(4,4'\text{-bpdo})_3(H_2O)_2](CF_3SO_3)_3\}_\infty \cdot 3H_2O$ (**4**)
Yellow crystals, Anal. Calc'd. (%) C 31.16, H 2.69, N 6.61, S 7.56; Found C 31.38, H 2.61, N 6.54, S 7.49 for $Yb_{0.5}Er_{0.5}C_{33}H_{34}N_6O_{20}F_9S_3$

$\{[Er(4,4'\text{-bpdo})_3(H_2O)_2](CF_3SO_3)_3\}_\infty \cdot 3H_2O$ (**5**)
Pale orange crystals, Anal. Calc'd. (%) C 31.23, H 2.70, N 6.62, S 7.58; Found C 31.30, H 2.42, N 6.55, S 7.97 for $Er_{1.0}C_{33}H_{34}N_6O_{20}F_9S_3$

2.3. Physical Characterisation

Elemental analyses (CHNS) were conducted by the Microanalytical Services Unit of the School of Chemistry and Molecular Biosciences, University of Queensland. Emission and excitation spectra were measured using a Horiba JY FluoroLog-311 spectrofluorimeter. For measurements in the Near Infra-Red (NIR) region, a liquid N_2 cooled InGaAs detector (DSS-IGA020L) was used, with excitation provided by a standard 450 W Xe arc lamp. For upconversion luminescence measurements in the visible region, a standard PMT (Hamamatsu R928P) detector was used with a 220 mW 980 nm CW diode laser (LQC980-220E) focused onto the sample as the excitation source. Upconverted emission was observed at 90° with respect to the direction of the laser diode propagation, with solid samples dispersed between two glass plates held at an incident angle of 60°. Variable excitation intensities were obtained using a continuously variable Neutral Density filter (NDC-50C-2, Thorlabs) placed in the excitation path, and were measured using a NIR power meter (Newport 1917-R), with specific care to ensure measurements were performed under identical conditions to power measurements.

2.4. X-ray Crystallography

Single-crystal X-ray Diffraction (SXRD) data were collected using an Oxford Diffraction Gemini CCD diffractometer, employing graphite monochromated Mo-K_α radiation (λ = 0.71073 Å), and operating in the ω-2Θ scan mode. An Oxford Cryosystems 600 series cryostream was used to maintain a constant temperature of 190 K during all data collection measurements. Data reduction and empirical absorption corrections (ψ-scans) were performed with the WINGX package.[27] Structures were solved by Direct Methods with SHELXS-86[28] and refined by full-matrix least squares analysis with SHELXL-2014.[29] All non-hydrogen atoms with occupancies greater than 0.5 were refined anisotropically. H atoms bonded to O or N atoms were located in the difference Fourier map before refinement. One of the triflate anions was found to be disordered over a special site, which required the use of fixed bond length (DFIX), fixed bond angle (DANG), and equivalent displacement parameter (EADP) restraints in order to facilitate realistic modelling. The position (EXYZ) and atomic displacement parameters (EADP) of metal cations for Yb_xEr_{1-x} heterobimetallic alloys were fixed to relative occupancies of the initially used stoichiometry. Molecular images were produced using Mercury (Version 3.5.1).[30]

3. Results and Discussion

3.1. Syntheses and Structural Studies

The 4,4'-bipyridine-N,N'-dioxide (4,4'-bpdo) ligand is easily prepared using well-known peracid oxidation techniques,[25] and the required Ln-based coordination polymers $\{[Ln_xLn_{1-x}(4,4'\text{-bpdo})_3(H_2O)_2](CF_3SO_3)_3\}_\infty$ (Ln = Yb and Er), as both homometallic ($x = 0$) and heterobimetallic ($1 > x > 0$) alloys, were readily synthesised herein under mild conditions using solvent diffusion mixture techniques. We have previously reported[31] the structure and luminescence properties of a high connectivity $(3^5.4^{14}.5^9)(3^5.4^{13}.5^{10})_2$ coordination polymer network, $[Yb(4,4'\text{-bpdo})_4](CF_3SO_3)_3]_\infty$, which form upon reaction of $Yb(CF_3SO_3)_3{\cdot}xH_2O$ with 4,4'-bpdo over a period of *ca.* 2-3 weeks using $CHCl_3$ as a chlorinated anti-solvent. In this case, using CH_2Cl_2 instead of $CHCl_3$, we initially observe formation of identical crystalline materials after 1-2 weeks, however upon prolonged complexation for an additional *ca.* 2-3 weeks, these crystals are quantitatively transformed into an alternative structure type that has also been previously characterised by Schroder et al[32] using $CHCl_3$. The resulting materials are coordination polymers with a $4^8.6^2$ 2D sheet network topology, which can be formulated as $[Yb(4,4'\text{-bpdo})_3(H_2O)_2](CF_3SO_3)_3]_\infty$, and also contain two bound inner sphere water molecules. Identical behaviour and products are observed when substituting Yb(III) for Er(III), and these observations suggest that the initial high connectivity networks are kinetic products, or alternately, that the slow ingress of water into the solvent mixture can influence the products obtained, which also illustrates the often dynamic nature of Ln(III) based MOF materials.[33]

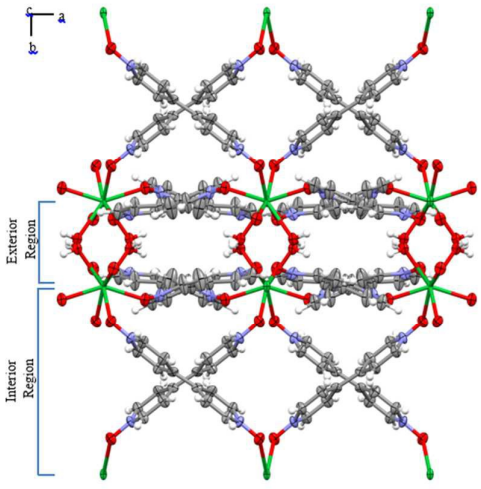

Figure 2. X-ray structure of $(4^8{\cdot}6^2)$ 2D coordination polymer network for $\{[Er(4,4'\text{-bpdo})_3(H_2O)_2](CF_3SO_3)_3\}_\infty$

In the present study, we focused on the preparation and characterisation of X-ray quality materials which contain two different lanthanide metal cations, but with identical coordination spheres in terms of the organic ligand (4,4'-bpdo) and coordinated or co-crystallised solvent molecules, in order to facilitate a comparison of the luminescence upconversion properties of the resulting coordination polymers. To that end, homometallic single metal complexes with Yb(III) (**1**) and Er(III) (**5**) were synthesised as controls together with a selection of heterobimetallic alloys containing *ca.* 5 %, 20 % and 50 % of Er(III) as a co-dopant (**2**-**4**).

Single-crystal X-ray diffraction studies reveal that the isolated crystals of **1**-**5** are isomorphous and isostructural, with a polymeric structure based on networks of eight coordinated lanthanide centres with approximate square anti-prismatic geometry, linked by 4,4'-bpdo ligands. The crystal structure that we obtain with Yb(III) is identical to that reported[32] by Schröder *et. al.* despite using a different chlorinated anti-solvent. The corresponding homometallic coordination polymer with Er(III) has not been previously reported. Recognising that the ionic radius of eight coordinate erbium and ytterbium differ only slightly by approximately 0.02 Å[34] due to the lanthanide contraction, it was satisfying to observe that the Er(III) complexes prepared under the same reaction conditions were essentially identical. For the Yb(III) compound, the isolated block-like crystals appeared yellow, while for Er(III), darker pale orange crystals were obtained.

A comparison of the crystallographic parameters for **1**-**5** is shown in Table 1, in order to elucidate further information concerning the properties of these materials. As shown, the unit cell tends to expand asymmetrically along the crystallographic *a*-axis with increasing percentage of Er(III) dopant. This may be attributed to the "spring-like" 4,4'-bpdo ligands, residing in the interior region of the 2D bilayer in the $4^8.6^2$ nets (see Fig. 2). As shown in Fig. 3a, when more erbium is doped into the complexes, the organic ligand can be twisted slightly allowing a stretch along the *a*-axis. A comparison of the average Ln-O bondlengths is also shown in Fig. 3b, with experimentally determined Ln-O bond distances showing an excellent agreement with expected values based on the percentage of incorporated Yb(III) and Er(III) cation. In all cases, the Ln–O bond distance increases when a larger percentage of Er(III) is present, which can be attributed to the slightly smaller ionic radius of the Yb(III) cation due to the well-known lanthanide contraction.[34]

Table 1. Summary of X-ray crystallographic data for isolated $\{[Yb_{1-x}Er_x(4,4'\text{-bpdo})_3(H_2O)_2](CF_3SO_3)_3\}_\infty$ coordination polymers (x = 0, 0.05, 0.2, 0.5, 1).

Complex	1	2	3	4	5
Empirical formula	$C_{33}H_{28}N_6O_{17}F_9S_3Yb_1$	$C_{33}H_{28}N_6O_{17}F_9S_3Yb_{0.95}Er_{0.05}$	$C_{33}H_{28}N_6O_{17}F_9S_3Yb_{0.8}Er_{0.2}$	$C_{33}H_{28}N_6O_{17}F_9S_3Yb_{0.5}Er_{0.5}$	$C_{33}H_{28}N_6O_{17}F_9S_3Er_1$
Temperature	293 (2)	293 (2)	293 (2)	293 (2)	293 (2)
Wavelength λ/ Å	0.71073	0.71073	0.71073	0.71073	0.71073
Crystal system	Orthorhombic	Orthorhombic	Orthorhombic	Orthorhombic	Orthorhombic
Space group	Pcca	Pcca	Pcca	Pcca	Pcca
a [Å]	16.7217 (7)	16.7310 (2)	16.7519 (3)	16.7521 (4)	16.7834 (5)
b [Å]	13.8732 (7)	13.8411 (4)	13.8277 (5)	13.8339 (4)	13.8374 (4)
c [Å]	20.1258 (9)	20.0979 (4)	20.0855 (5)	20.0849 (4)	20.1138 (4)
α = β = γ [°]	90	90	90	90	90
V [Å]	4668.85 (4)	4654.18 (2)	4652.63 (2)	4654.63 (2)	4671.20 (2)
Z	4	4	4	4	4
D_{calcd} [g cm^{-3}]	1.74	1.74	1.74	1.74	1.73
Reflections collected	10357	14625	16699	16535	14496
wR_2	0.1936	0.1320	0.1451	0.1267	0.1523
R_{obs}, R_{all}	0.0590, 0.1002	0.0468, 0.0701	0.0509, 0.0787	0.0448, 0.0636	0.0521, 0.0792

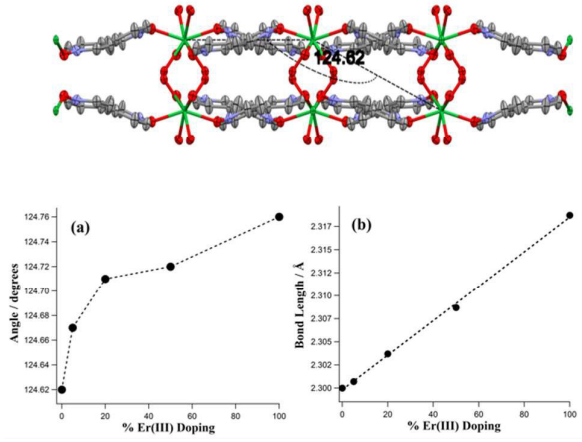

Figure 3. Comparison of selected bond angle (shown for **1**) along the *a*-axis and average Ln-O bondlength as a function of doped %Er(III) in $\{[Yb_{1-x}Er_x(4,4'\text{-bpdo})_3(H_2O)_2](CF_3SO_3)_3\}_\infty$ coordination polymers.

3.3. Photoluminescence

We have previously shown[31] that 4,4'-bpdo acts as a light harvesting antennae for sensitised Ln(III) emission, and solid state Near Infra-Red (NIR) emission spectra of **1-5** have been measured upon 360 nm excitation in the solid state at room temperature (see Fig. S1, Supp. Info). The characteristic $^2F_{5/2} \rightarrow {}^2F_{7/2}$ and $^4I_{13/2} \rightarrow {}^4I_{5/2}$ emission bands of the Yb(III) and Er(III) cations respectively are clearly observed at *ca*. 980 and 1540 nm, with relative emission intensities that vary in accordance with the differing mole fraction of each cation. Corresponding excitation spectra were also measured (see Fig S2, Supp. Info.) for **1-4** monitoring the NIR emission of Yb(III) at 980 nm, and for **5** monitoring the Er(III) emission at 1520 nm. These spectra show an excitation peak at *ca*. 360 nm in the UV region, agreeing with our previously assigned absorption[31] of the 4,4'-bpdo ligand.

Given their predictable structural behaviour observed using X-ray studies, we were interested in the potential of the developed $\{[Yb_{1-x}Er_x(4,4'\text{-bpdo})_3(H_2O)_2](CF_3SO_3)_3\}_\infty$ coordination polymers to demonstrate upconversion luminescence behaviour. Hence, the emission spectra obtained upon 980 nm excitation were measured, and the resulting spectrum for 5% Er(III) dopant is shown as an example in Fig. 4, where sharp upconverted emission peaks spanning the visible region and extending into the UV region are observed. A relatively weak red emission band at 660 nm can be attributed to the $^4F_{9/2} \rightarrow {}^4I_{15/2}$ transition of the Er(III) cation, while much more intense green emission bands centered at 548 nm and 525 nm can be ascribed to $^4S_{3/2} \rightarrow {}^4I_{15/2}$ and $^2H_{11/2} \rightarrow {}^4I_{15/2}$ transitions respectively. Importantly, these peaks show evidence of splitting due to crystal field effects, and the green emission is clearly evident, even with the naked eye, and can be measured with an excitation laser power as low as *ca*. 10 mW. At higher energy, a blue emission band at 409 nm is also observed, corresponding to the $^2H_{9/2} \rightarrow {}^4I_{15/2}$ transition. Most interestingly, we also observe two rarely reported emission bands in the blue and UV regions, centered at 455 nm and 380 nm. An examination of the energy level structure for Er(III) reveals these bands can be attributed to $^4F_{5/2} \rightarrow {}^4I_{15/2}$ and $^4G_{11/2} \rightarrow {}^4I_{15/2}$ transitions respectively.

The latter peak has been observed previously in mixed metal nanoparticle systems[12-13,35] such as $NaY(Ln)F_4$, but to the best of our knowledge, this emission has not been reported in a lanthanide based coordination polymer. We also note that the strong intensity of the Er(III) emission allows us to clearly resolve several crystal field splitting peaks, which are otherwise rarely reported in the literature.[17-24]

3.4. Upconversion Properties

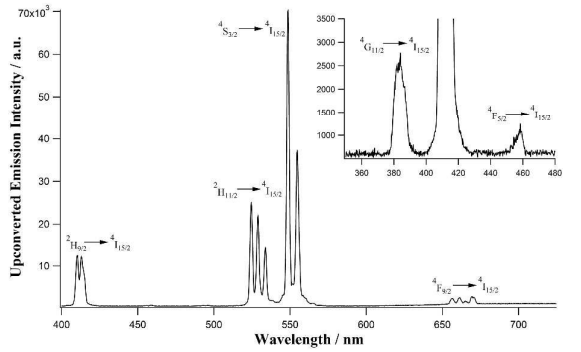

Figure 4. Visible upconversion emission spectrum of 5% Er(III) dopant upon 980 nm excitation (laser power = 200 mW). Inset: expansion of the UV region.

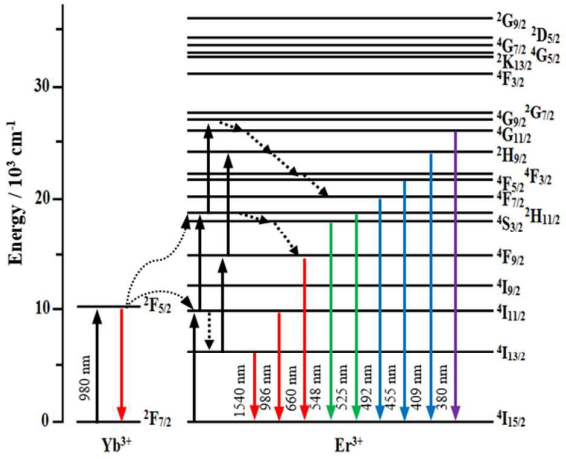

Figure 5. Energy level diagram showing upconverted Er(III) emission upon 980 nm excitation of Yb(III) sensitiser.

3.4.1. Power Dependence and Saturation Effects

In order to further characterise the luminescence upconversion mechanism, an input power dependence study of the emission intensities was undertaken at room temperature. The upconverted emission intensity (I) of the four major transitions in the visible region were measured as a function of the input pump power (P). Typically, for the upconversion process, I is proportional to the nth power of P, i.e. $I \propto P^n$, where n is the number of excited photons required to populate the higher energy levels of the emitting ion.[36] Hence, a plot of log(I) versus log(P) should give a straight line with slope n. As shown in Fig. 6a, the slopes n of the 5% Er(III) doped heterobimetallic complexes upon low pump power (>50 mW) excitation for the 409 nm, 525 nm, 548 nm and 660 nm emission bands are *ca.* 3, 2, 2 and 2 respectively. These results indicate that a three-photon excitation process is responsible for the blue emission, while two-photon excitation processes are responsible for the green and red emissions bands. As the input pump power is increased, saturation takes place and the slopes n for the 20 % and 50 % Er(III) doped heterobimetallic compounds clearly decrease to approximately 1 (Fig. 6b & 6c).

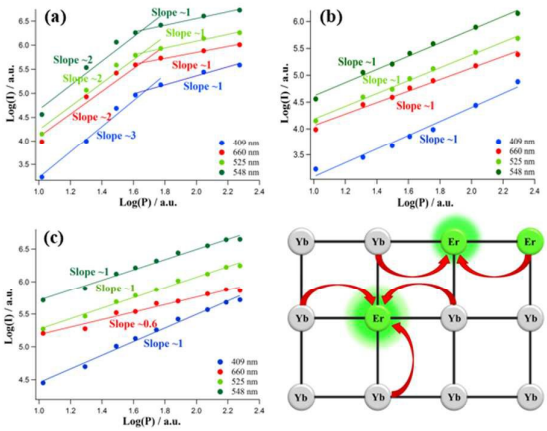

Figure 6. Power dependence of emission intensities for blue, green and red emission of $\{[Yb_{1-x}Er_x(4,4'\text{-bpdo})_3(H_2O)_2](CF_3SO_3)_3\}_\infty$ coordination polymers with (a) $x = 0.05$, (b) $x = 0.2$, and (c) $x = 0.5$ upon 980 nm laser excitation. Bottom right: Illustration of energy transfer upconversion (ETU) mechanism responsible for the emission.

There are two well-known upconversion mechanisms responsible for luminescence, which are specifically excited-state absorption (ESA) and energy-transfer-upconverison (ETU) processes.[37-39] The results from our power dependence study indicate that the observed upconversion changes from a predominantly ESA to ETU mechanism as the percentage of Er(III) doping is increased, which is in agreement with results previously reported using a Yb^{3+}/Er^{3+} co-doped Gd_2O_3 nanophosphor.[39]

4. Conclusions

A series of Yb^{3+}/Er^{3+} co-doped coordination polymers were synthesised under mild conditions and fully characterised using X-ray diffraction techniques. The characteristic photoluminescence properties of the Yb(III) and Er(III) cations in the NIR were compared upon 360 nm excitation. Moreover, the upconversion properties of this series were also compared upon excitation in the NIR at 980 nm, showing intense emission in the blue, green and red region of the visible spectrum, and a weaker emission peak also extending into the UV region. Despite the presence of two inner sphere water molecules, which typically quench Ln(III) based NIR emission,[40] our results demonstrate that this deactivation pathway may be of less importance for upconverted emission in the visible region, and the development of Ln(III) based coordination polymers is likely an underexplored research area. Indeed, it is also possible that the presence of low energy phonon modes may assist visible upconversion, by facilitating non-radiative internal conversion within the excited state manifold of Er(III), and we are pursuing the synthesis of selectively deuterated samples to explore this possibility.

5. Acknowledgements

Financial support by the Australian Research Council (ARC-FT100100795) is gratefully acknowledged.

6. Notes and References

[1] A. Yella; H.-W. Lee; H. N. Tsao; C. Yi; A. K. Chandiran; M. K. Nazeeruddin; E. W.-G. Diau; C.-Y. Yeh; S. M. Zakeeruddin and M. Graetzel, *Science*, **2011**, *334*, 629.
[2] M. A. Green; K. Emery; Y. Hishikawa; W. Warta and E. D. Dunlop, *Prog. Photovoltaics Res. Appl.*, **2015**, *23*, 1.
[3] K. Masuko; M. Shigematsu; T. Hashiguchi; D. Fujishima; M. Kai; N. Yoshimura; T. Yamaguchi; Y. Ichihashi; T. Mishima; N. Matsubara; T. Yamanishi; T. Takahama; M. Taguchi; E. Maruyama and S. Okamoto, *IEEE J. Photovolt.*, **2014**, *4*, 1433.
[4] M. A. Green; K. Emery; Y. Hishikawa; W. Warta and E. D. Dunlop, *Prog. Photovoltaics Res. Appl.*, **2012**, *20*, 606.
[5] C. Gueymard, *Sol. Energy*, **2004**, *76*, 423.
[6] B. S. Richards, *Sol. Energy Mater. Sol. Cells*, **2006**, *90,* 2329.
[7] J. de Wild; A. Meijerink; J. K. Rath; W. G. J. H. M. van Sark and R. E. I. Schropp, *Energy Environ. Sci.*, **2011**, *4*, 4835.
[8] S. Sanders, R. G. Waarts, D. G. Mehuys and D. F. Welch., *Appl. Phys. Lett.*, **1995**, 67, 1815.
[9] E. W. Barrera; M. C. Pujol; F. Diaz; S. B. Choi; F. Rotermund; K. H. Park; M. S. Jeong and C. Cascales, *Nanotechnology*, **2011**, *22*, 075205.
[10] J. Chen and J. X. Zhao, *Sensors*, **2012**, *12*, 2414.
[11] T. F. Schulze and T. W. Schmidt, *Energy Environ. Sci.*, **2015**, *8*, 103.
[12] S. Mishra; G. Ledoux; E. Jeanneau; S. Daniele and M.-F. Joubert, *Dalton Trans.*, **2012**, 41, 1490.
[13] I. Recalde; N. Estebanez; L. Francés-Soriano; M. Liras; M. González-Béjar and J. Pérez-Prieto, *Nanoscale*, **2016**, 8, 7588.
[14] J. Rocha; L. D. Carlos; F. A. A. Paz and D. Ananias, *Chem. Soc. Rev.*, **2011**, 40, 926.
[15] Y. Cui; B. Chen and G. Qian, *Coord. Chem. Rev.*, **2014**, 273-274, 76.
[16] Y. Hasegawa and T. Nakanishi, *RSC Adv.*, **2015**, 5, 338.
[17] K. L. Wong; W. M. Kwok; W. T. Wong; D. L. Philips and K. W. Cheah, *Angew. Chem. Int. Ed.*, **2004**, *43*, 4659.
[18] K. L. Wong; G. L. Law; W. M. Kwok; W. T. Wong and D. L. Philips, *Angew. Chem. Int. Ed.*, **2005**, 44, 3436.
[19] D. Weng; X. Zheng and L. Jin, *Eur. J. Inorg. Chem.*, **2006**, 4184.
[20] J. Yang; Q. Yue; G.-D. Li; G.-H. Li; J.-S. Chen, *Inorg. Chem.*, **2006**, 45, 2857.
[21] D. Weng; X. Zheng; X. Chen; L. Li and L. Jin, *Eur. J. Inorg. Chem.,* **2007**, 3410.
[22] P. Mahata; K. V. Ramya and S. Natarajan, *Dalton Trans.*, **2007**, 36, 4017
[23] P. Mahata; K V. Ramya and S. Natarajan, *Chem. Eur. J.*, **2008**, 14, 5839.
[24] C.-Y. Sun; X.-J. Zheng; X.-B. Chen; L.-C. Li and L.-P. Jin, *Inorg. Chim. Acta*, **2009**, *362*, 325.
[25] J. Jia, A. J. Blake, N. R. Champness, P. Hubberstey, C. Wilson and M. Schröder, *Inorg. Chem.*, **2008**, 47, 8652
[26] D.-L. Long; A. J. Blake; N. R. Champness; C. Wilson and M. Schröder, *Chem. Eur. J.*, **2002**, *8*, 2026.
[27] L. J. Farrugia, *J. Appl. Crystallogr.*, **1999**, *32*, 837.
[28] G. M. Shledrick, *SHELXS86 - Program for Crystal Structure solution*, Institüt für Anorganische Chemie der Universität, Tammanstrasse 4, D-3400 Göttingen, Germany, **1986**.
[29] G. M. Sheldrick, *SHELX-2014: Programs for Crystal Structure Analysis*, University of Göttingen, Göttingen, **2014**.
[30] C. F. Macrae, P. R. Edgington, P. McCabe, E. Pidcock, G. P. Shields, R. Taylor, M. Towler and J. Van de Streek, *J. Appl. Crystallogr.*, **2006**, *39*, 453.
[31] G. M. Sequira; W. Y. Tan and E. G. Moore, *Dalton Trans*., **2015**, *44*, 13378.
[32] R. J. Hills; D.-L Long; M. S. Turvey; A. J. Blake; N. R. Champness; P. Hubberstey; C. Wilson and M. Schröder*, Chem. Commun.*, **2004**, 1792.
[33] T. Kowall; F. Foglia; L. Helm and A. E. Merbach, *Chem. Eur. J.*, **1996**, *2*, 285.
[34] M. Seitz; A. G. Oliver and K. N. Raymond, *J. Am. Chem. Soc.*, **2007**, 129, 11153.
[35] A. K. Singh; P. K. Shahi; S. B. Rai and B. Ullrich, *RSC Adv.*, **2015**, 5, 16067.
[36] M. Pallnau; D. R. Gamelin; S. R. Lüthi and H. U. Güdel, *Phys. Rev. B*, **2000**, 61, 3337.
[37] H. Lin; G. Meredith; S. Jiang; X. Peng; T. Luo; N. Peyghambarian and E. Y.-B. Pun, *J. Appl. Phys.,* **2003**, ***93***, 186.
[38] H. Guo; N. Dong; M. Yin; W. P. Zhang; L. R. Lou and S. D. Xia, *J. Alloys Compd.*, **2006**, *415*, 280.
[39] S. K. Singh; K. Kumar and S. B. Rai, *Appl. Phys. B*, **2009**, *94*, 165.
[40] S. Faulkner; A. Beeby; R. S. Dickins; D. Parker and J. A. G. Williams, *J. Fluoresc.*, **1999**, *9*, 45.

